Letters

A Noninvasive Feeder Impedance Estimation Method for Parallel Inverters in Microgrid Based on Load Harmonic Current

Baojin Liu, *Member, IEEE*, Zeng Liu, *Member, IEEE*, and Jinjun Liu, *Fellow, IEEE*

***Abstract*—As a key parameter in microgrids, feeder impedance is closely related to power distribution, power quality, and system stability. This letter proposes a novel noninvasive feeder impedance estimation method, which uses the microgrid central controller (MGCC) and inherent harmonic signals introduced by a nonlinear or unbalanced load. First, the sequence impedance model for a droop-controlled inverter is built to demonstrate that the inverter output impedance is negligible at low-order harmonic frequencies. Then, the bus voltage and output current at a specific dominant harmonic frequency are extracted in MGCC, based on which feeder impedance can be obtained. Finally, the estimated feeder impedance is used to generate proper virtual impedance to enhance power sharing and voltage quality as an example, based on a hierarchical control structure. Experimental results are provided to validate the proposed method.**

***Index Terms*—Hierarchical control, impedance estimation, microgrid, power sharing, voltage distortion.**

I. Introduction

RECENTLY, distributed generation (DG) integrated with renewable energy resources has become increasingly attractive. A DG unit is typically connected to the point of common coupling (PCC) with power electronics-based interfaces (e.g., inverters) such that the coordinative control of parallel-connected inverters is imperative for robust operation. A microgrid consists of a cluster of DG units and can operate in islanded and grid-connected modes to feed critical loads flexibly and reliably. To realize adequate load power sharing and high-quality power supply in the microgrid, a hierarchical control structure consisting of primary control, secondary control, and tertiary control has been proposed and widely applied in microgrid control [1]. The real power frequency (P-ω) and reactive power amplitude (Q-V) droop based primary control is implemented in inverter local controllers, and has been deemed superior given the capacity for power sharing without communication [2].

Manuscript received October 4, 2020; revised November 13, 2020; accepted November 30, 2020. Date of publication December 9, 2020; date of current version March 5, 2021. This work was supported by the National Natural Science Foundation of China under Grant 51777160. *(Corresponding author: Zeng Liu.)*

The authors are with the State Key Lab of Electrical Insulation and Power Equipment, School of Electrical Engineering, Xi'an Jiaotong University, Xi'an 710049, China (e-mail: liubaojin.pe@gmail.com; zengliu@xjtu.edu.cn; jjliu@xjtu.edu.cn).

Color versions of one or more of the figures in this article are available online at https://doi.org/10.1109/TPEL.2020.3042700.

Digital Object Identifier 10.1109/TPEL.2020.3042700

Secondary and tertiary controls are usually applied in microgrid central controller (MGCC) to achieve power quality control and system optimization. The information exchange between inverter local controller and MGCC is realized via communication links [1].

Despite accurate real power sharing, self-synchronization, and communication-free feature, traditional droop control has several limitations, including power control coupling, unequal reactive/unbalanced/harmonic power sharing, and PCC voltage distortion, which are each related to feeder impedance [3]. Moreover, feeder impedance is a necessary parameter in system modeling and analysis, islanding and fault detection, system monitoring, and other applications [4]; the feeder impedance estimation method (FIEM) thus warrants in-depth study.

Depending on whether extra perturbation is injected, existing FIEMs can be classified as either invasive [5]–[8] or noninvasive [4], [9]–[12]. Invasive methods deliberately inject a disturbance signal into the system via the inverter or a dedicated device and then estimate impedance based on the response. Accurate results can be acquired because the signal-to-noise ratio (SNR) is generally high; however, the system is vulnerable to extra disturbance. The noninvasive methods introduced in [4], [9], and [10] use background signals inherently presented in the system to estimate impedance without extra disturbance, but they are only applicable to single-inverter grid-connected systems. Moreover, noninvasive approach discussed in [11] calculates feeder impedance for parallel-inverter systems based on extended Kalman filter (EKF) and PCC voltage sampling. On one hand, tuning EKF covariance matrix is very difficult; on the other hand, the FIEM in [11] relies on the synchronous sampling of inverter terminal voltage and PCC voltage, where high-speed communication links seeding PCC voltage to each inverter are unavoidable. Moffat *et al.* [12] propose a noninvasive method which is applicable not only to parallel-inverter systems, but also to more complicated topologies, e.g., networked system. Unfortunately, signal sampling based on synchrophasor measurement units at each node is required, which dramatically increases the cost.

To tackle aforementioned limitations in existing FIEMs, this letter proposes a noninvasive FIEM for parallel inverters in the microgrid under the premise of using the inherent harmonic signals introduced by a nonlinear or unbalanced load and calculating the impedance in MGCC, where there is no extra need on

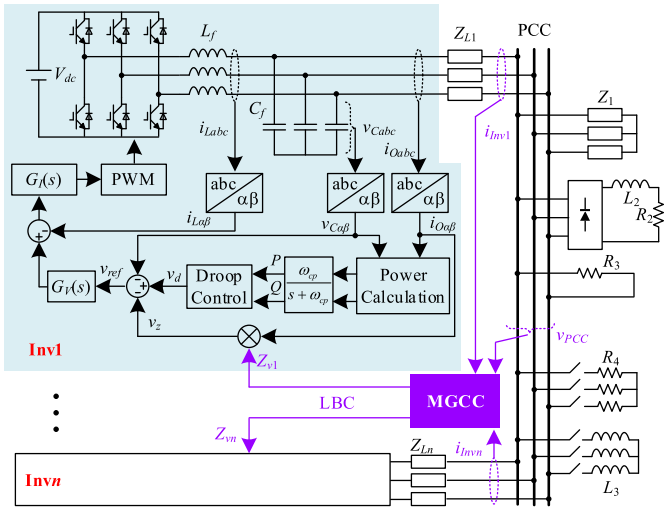

Fig. 1. Microgrid structure with multiple parallel-connected inverters.

disturbance, sensors, or communication. The remainder of this letter is organized as follows. Section II describes the proposed FIEM in detail. Section III provides a sample application of feeder impedance. In Section IV, experimental results are presented to verify the proposed method. Finally, the conclusion is given in Section V.

II. Proposed Noninvasive Feeder Impedance Estimation Method

A traditional ac microgrid consists of multiple inverters connected in parallel as shown in Fig. 1. Feeder impedance differs based on distributed feature and can be considered constantly inductive—resistive at low-frequency ranges in a low-voltage network. Various load types may exist, including balanced, unbalanced, and nonlinear forms. Unbalanced loads absorb fundamental negative sequence-current from the system, and nonlinear loads absorb harmonic current.

A. Droop Control and Equivalent Circuit Analysis

To realize automatic power sharing without communication, droop control is adopted as shown in the following:

$$\begin{cases} \omega^* = \omega_0 - k_p P \\ V^* = V_0 - k_q Q \end{cases} \tag{1}$$

where ω^* and ω_0 denote the reference and nominal frequency, respectively; V^* and V_0 are the reference and nominal amplitude, respectively; and k_p and k_q are each droop coefficients. Virtual impedance is often incorporated by subtracting the virtual voltage drop from the voltage reference to further improve control performance (e.g., power decoupling and power sharing). Regarding the inner loop, the voltage controller in proportional resonant form and current controller in proportional form are commonly used to track the voltage reference and ensure internal stability. The expressions of voltage and current controllers are

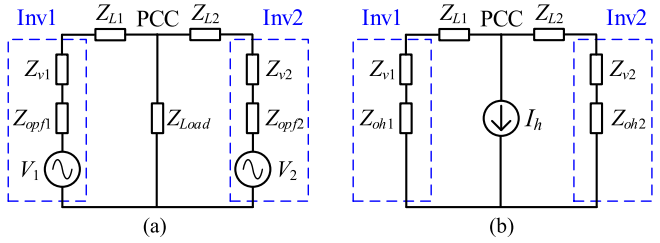

Fig. 2. Equivalent circuit of two-parallel-inverter system at (a) fundamental positive sequence and (b) harmonic frequencies.

shown in the following:

$$G_V(s) = k_{pV} + \sum_{h=1,5,7,11} \frac{2k_{ih}\omega_c s}{s^2 + 2\omega_c s + (h\omega^*)^2} \tag{2}$$

$$G_I(s) = k_{pI} \tag{3}$$

where $G_V(s)$ and $G_I(s)$ are the transfer functions of voltage and current controllers, respectively; k_{pV} is the gain of voltage proportional controller; k_{ih} is the gains of each resonant controller; ω_c is the cutoff frequency of the resonant controllers; and k_{pI} is the gain of current proportional controller. All the above functions are realized in the local controller of each inverter based on local variables. Furthermore, MGCC is usually installed at PCC to realize secondary control or other ancillary functions and to send control commands to the local controller via low-bandwidth communication (LBC) according to the PCC voltage and output current of each inverter.

Taking a two-parallel-inverter system as an example, the droop-controlled inverter can be represented by a controlled voltage source, whose amplitude and frequency references are given in (1). Accordingly, the equivalent circuit at fundamental positive sequence is illustrated in Fig. 2(a), where V_i ($i = 1$, 2, hereafter) is the fundamental voltage, Z_{opfi} is the inverter output impedance at fundamental positive sequence, Z_{vi} is the virtual impedance, Z_{Li} is the feeder impedance, and Z_{Load} is the lumped PCC load. However, the inverter acts as a short circuit at harmonic frequencies (including fundamental negative sequence hereafter), as the reference voltage is purely sinusoidal in positive sequence. The equivalent circuit at harmonic frequencies is shown in Fig. 2(b), where Z_{ohi} is the inverter output impedance at harmonic frequencies, nonlinear loads are represented by a lumped harmonic current source I_h.

B. Sequence Impedance Model of Droop-Controlled Inverter

To evaluate the impact of Z_{ohi}, the sequence impedance model of a droop-controlled inverter is built following similar theory as in [13]. The modeling process will not be introduced due to page limits, but expressions for positive and negative sequence impedance appear in the Appendix, and their bode plots with simulated results are shown in Fig. 3 by using the parameter in Table I. The simulated results accord well with the model, whose accuracy can thus be verified. The sequence impedance varies along with the droop coefficient k_p and the cutoff frequency of the low-pass filter (LPF) ω_{cp} as illustrated in Fig. 4. However, only positive sequence impedance around 50 Hz is affected by

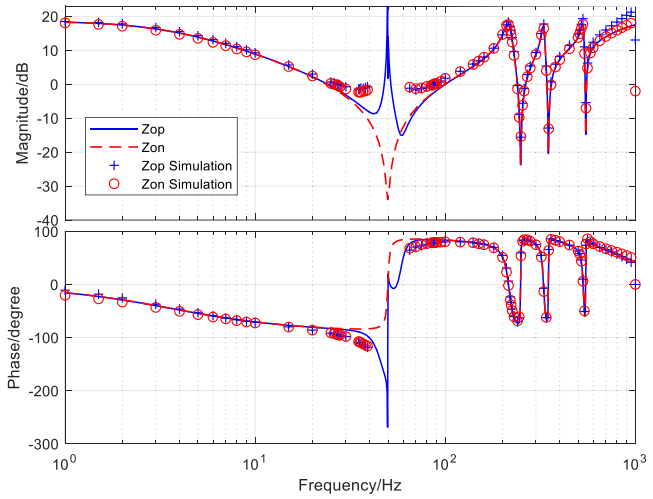

Fig. 3. Sequence impedance of droop-controlled inverter and its simulation measurement results.

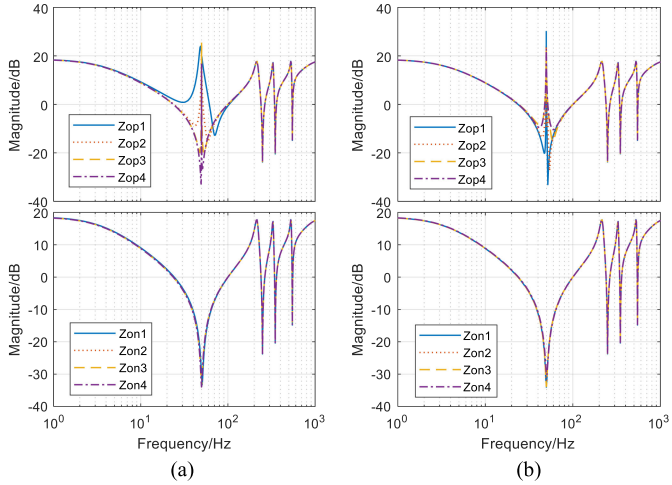

Fig. 4. Variation of sequence impedance magnitude along with k_p and ω_{cp}. (a) $k_p = 6.28\text{e}-3, 6.28\text{e}-4, 6.28\text{e}-5, 6.28\text{e}-6$, respectively; (b) $\omega_{cp} = 0.62$, 6.2, 62, 620, respectively.

TABLE I
EXPERIMENT PARAMETERS

Symbol	Description	Value
V_{dc}	DC voltage (V)	600
f_s	Switching frequency (kHz)	12.5
S	Capacity of each DG (kVA)	9
L_f	Filter inductance (mH)	3
C_f	Filter capacitance (μF)	30
k_p	P-ω droop gain (rad/s/W)	3.14e-4
k_q	Q-V droop gain (V/var)	5e-4
ω_0	Nominal angular frequency (rad/s)	100π
V_0	Nominal phase voltage amplitude (V)	163
ω_{cp}	Cutoff frequency of LPFs for power calculation (rad/s)	31
Z_e	Expected equivalent impedance (mH+Ω)	1.05+0.25
Z_1	Balanced linear load (mH+Ω)	50+70
L_2	Nonlinear load inductance (mH)	6
R_2	Nonlinear load resistance (Ω)	40
R_3	Single-phase load resistance (Ω)	40
R_4	Resistive load disturbance (Ω)	175
L_3	Inductive load disturbance (mH)	50

the droop control. It can also be observed that the magnitude of output impedance at –1st-order harmonic frequency is about –35 dB; at ±5th-order harmonic frequency is about –25 dB; at ±7th-order harmonic frequency is about –20 dB; and at ±11th-order harmonic frequency is about –15 dB. Compared with feeder impedance, the magnitude of output impedance at low-order harmonic frequencies, i.e., Z_{oh}, can be neglected [2].

C. Principle of the Proposed Noninvasive FIEM

According to Fig. 2(b), when Z_{ohi} is neglected and Z_{vi} is set to zero, only feeder impedance Z_{Li} is present in each inverter branch; therefore, Z_{Li} can be easily calculated with Ohm's law if the harmonic component of PCC voltage and the inverter output current are measured. Considering that the MGCC originally measures the PCC voltage and output current of each inverter

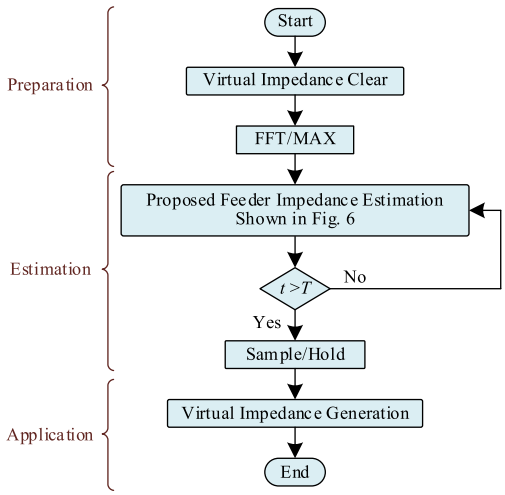

Fig. 5. Operation flowchart of the proposed FIEM.

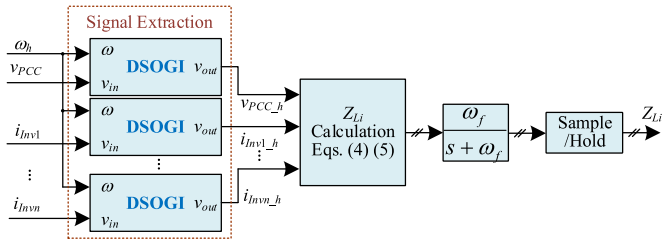

Fig. 6. Operation principle of the proposed FIEM.

for monitoring and protection purposes, the proposed noninvasive FIEM is performed in MGCC by following the procedure illustrated in Fig. 5, and the estimation principle is shown in Fig. 6.

During the preparation process in Fig. 5, zero virtual impedance command is sent from MGCC to inverter local controllers to avoid the influence of virtual impedance. Afterward, system identification is conducted based on FFT analysis of PCC voltage to determine the harmonic order applied in the

proposed FIEM (represented by h). Theoretically, any low-order harmonics due to nonlinear loads could potentially be used to calculate Z_{Li}. However, selecting the dominant order with maximum amplitude can provide a better SNR and more accurate results. Typically, the –1st- and the –5th-order harmonics are preferred candidates in this FIEM.

The estimation process shown in Fig. 6 is triggered after the preparation process. To extract the hth harmonic voltage and current component, the DSOGI based signal extraction method proposed in [14] is adopted. The DSOGI is basically a band pass filter which only allows the signal at resonant frequency ω_h to pass. Then the feeder impedance of inverter i can be calculated in the stationary frame ($\alpha\beta$ frame) by the following equations based on the extracted harmonic signals:

$$R_{Li} = -\frac{v_{\mathrm{PCC}\_h\alpha} i_{\mathrm{Inv}i\_h\alpha} + v_{\mathrm{PCC}\_h\beta} i_{\mathrm{Inv}i\_h\beta}}{i^2_{\mathrm{Inv}i\_h\alpha} + i^2_{\mathrm{Inv}i\_h\beta}} \tag{4}$$

$$L_{Li} = \frac{v_{\mathrm{PCC}\_h\beta} i_{\mathrm{Inv}i\_h\alpha} - v_{\mathrm{PCC}\_h\alpha} i_{\mathrm{Inv}i\_h\beta}}{\left(i^2_{\mathrm{Inv}i\_h\alpha} + i^2_{\mathrm{Inv}i\_h\beta}\right)\omega_h} \tag{5}$$

where R_{Li} and L_{Li} are the feeder resistance and inductance, respectively; $v_{\mathrm{PCC}\_h\alpha}$ and $v_{\mathrm{PCC}\_h\beta}$ denote the extracted hth harmonic voltage in the $\alpha\beta$ frame; $i_{\mathrm{Inv}i\_h\alpha}$ and $i_{\mathrm{Inv}i\_h\beta}$ are the extracted hth harmonic current of inverter i in the $\alpha\beta$ frame; and ω_h is the angular frequency of the hth-order harmonic.

Next, the measured Z_{Li} is passed through an LPF to remove measurement noise, whose cutoff frequency ω_f is 10 rad/s in this letter. The final estimation result can be held in MGCC once $t > T$, where T is a predetermined timer. Based on the experience, the estimation process takes about several seconds, the timer T can be designed accordingly. Since the feeder impedance does not change frequently, the FIEM algorithm can cease operating when the whole estimation process is completed, and the feeder impedance can be used in the following application process.

Two things need to be clarified regarding the proposed FIEM. First, the discussion above assumes all the nonlinear loads are installed at PCC to simplify the discussion. In practical microgrids, it is likely that some nonlinear loads are installed near by the inverters. In this case, the proposed FIEM can still work normally due to the following two reasons. On one hand, the inverter output impedance is much smaller than the feeder impedance according to the analysis in Section II-B; on the other hand, the harmonic current of local loads is unlikely to be much larger than the harmonic current of PCC load. Therefore, the voltage drop on inverter output impedance can still be ignored, and the feeder impedance can be accurately obtained even when there exist local nonlinear loads. Second, this letter takes the droop control shown in (1) as an example to show the basic idea and analysis methodology. Actually, the proposed FIEM is applicable to parallel-inverter system under other forms of droop control or even virtual synchronous generator (VSG) control, as long as the inverter is controlled as voltage source, and its output impedance at low-order harmonic frequencies is small enough.

Compared with existing FIEMs, the proposed method offers three advantages. First, it is noninvasive; all the harmonic signals, MGCC, and PCC voltage and current sampling are inherently presented in the system. Second, its measurement accuracy and SNR are high because the harmonic signals associated with nonlinear loads usually have a larger amplitude than injected perturbations under invasive methods. Finally, the proposed FIEM only requires PCC signals; therefore, communication or multi-point synchronous sampling is not needed. One limitation involves the dependence of unbalanced loads or nonlinear loads, which should not be of concern in a modern microgrid with massive power-electronic loads.

III. Application to Enhance Power Sharing and Voltage Quality

Once the feeder impedance has been obtained, it can be used to solve many issues in the field of microgrid control. A direct way to enhance power sharing and voltage quality based on feeder impedance is introduced in this section as an example.

It is well known that traditional droop control is incapable of reactive power, unbalanced power, or harmonic power sharing [2]. Based on the equivalent circuit depicted in Fig. 2, power-sharing error is determined by the feeder impedance difference. If the equivalent impedance defined in (6) of each inverter branch is compensated to a common value by introducing proper virtual impedance, the power sharing can be enhanced. Now that Z_{Li} has been estimated, the virtual impedance for each inverter can be easily obtained if Z_e is determined

$$Z_{ei} = Z_{vi} + Z_{Li}. \tag{6}$$

As for PCC voltage quality, it may degrade when feeding nonlinear loads because the inner voltage loop only controls the inverter's terminal voltage. According to Fig. 2(b), the harmonic components in PCC voltage are proportional to Z_e when feeding a certain extent of nonlinear load. In other words, the total harmonic distortion (THD) of PCC voltage is positively correlated with Z_e. Therefore, the THD of PCC voltage will be suppressed if Z_e is designed to be smaller than the original feeder impedance (Z_{vi} is a negative value in this case). Nevertheless, the system may become unstable if Z_e is too small; there exists a tradeoff between PCC voltage distortion and system stability. The design of Z_e is beyond the scope of this letter but can be selected according to [15]. Once Z_e has been determined, the virtual impedance for each inverter can be obtained in MGCC by comparing Z_{Li} with Z_e. Afterward, the Z_{vi} command is sent to the local controller of the corresponding inverter via LBC.

The overall operating process can be summarized as follows. The microgrid starts with the proposed FIEM and traditional droop control without virtual impedance, during which the feeder impedance can be estimated. Then the virtual impedance is generated and transmitted to each inverter. Once all inverters acknowledge the receipt of Z_v command, the MGCC and LBC can stop running, and will restart only when the system configuration changes. Feeder impedance can be discerned using this method. Additionally, the load power can be shared equally, and the THD of PCC voltage can be reduced. Although the proposed method relies on MGCC and LBC, system reliability will not deteriorate: the system only runs intermittently for a short time, and the requirement for LBC is very low; only a complex constant value is transmitted in a unidirectional manner.

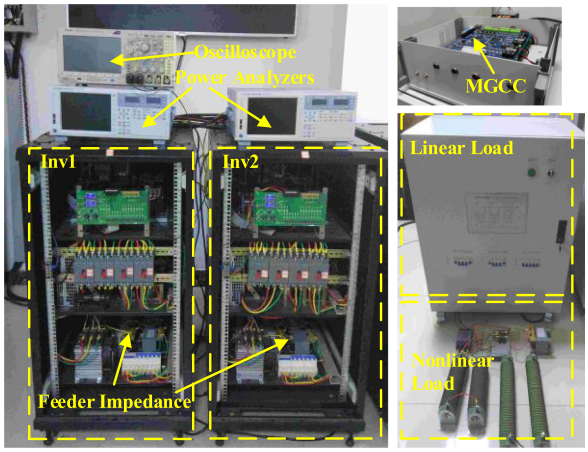

Fig. 7. Photograph of the experimental platform.

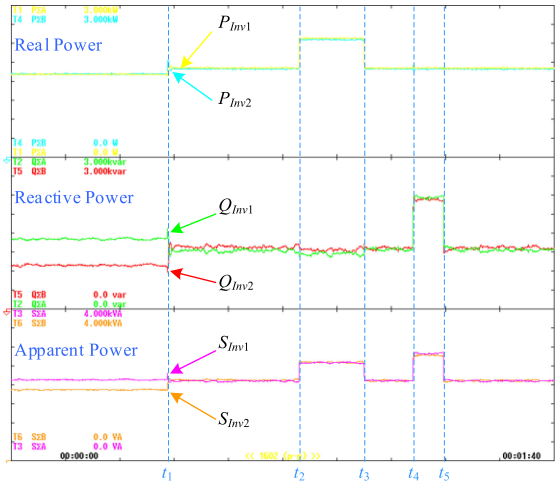

Fig. 8. Experimental waveforms of real power, reactive power, and apparent power for both inverters, virtual impedance was introduced at t_1, resistive load step changed at t_2 and t_3, and inductive load step changed at t_4 and t_5.

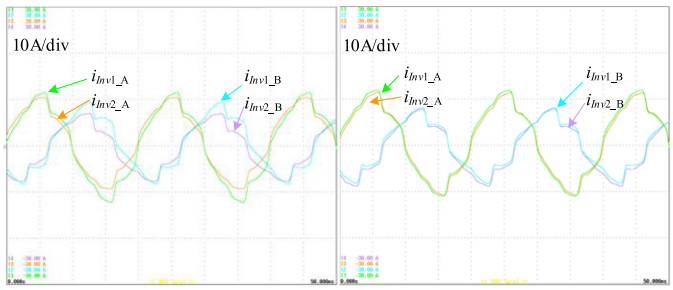

(a) (b)

Fig. 9. Experimental waveforms of phase-A and phase-B output current for both inverters, (a) before and (b) after virtual impedance is introduced.

IV. Experimental Results

To verify the proposed FIEM and its application method, experiments based on the platform presented in Fig. 7 have been conducted. The platform contained two inverters, balanced load, unbalanced load, nonlinear load, and MGCC, connected via topology similar to that in Fig. 1. Each inverter was composed of a three-phase three-leg bridge, an *LC* filter, and feeder impedance. Detailed power-stage and control parameters are given in Table I. All control algorithms in inverter local controllers and MGCC were realized through DSP TMS320F28335 from Texas Instruments. One power analyzer (YOKOGAWA WT1804E) was used to measure the output power, inverter current, and PCC voltage. The –5th-order harmonic was selected in the FIEM, and the CAN protocol was utilized as LBC. The experiment was run following the process described in Fig. 5. Then, resistive and inductive load step changes were performed to further verify the approach's effectiveness.

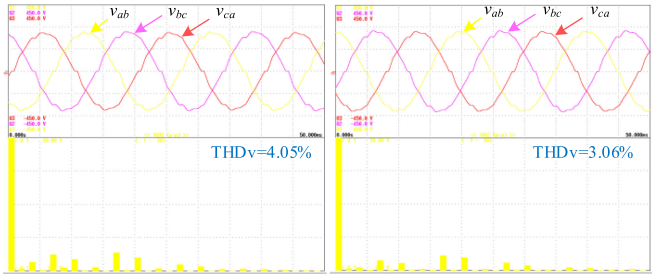

(a) (b)

Fig. 10. Waveforms and THD analysis of PCC voltage (a) before and (b) after virtual impedance is introduced.

TABLE II
Feeder Impedance Estimation Results

	Resistance (Ω)		Inductance (mH)	
	Inv1	Inv2	Inv1	Inv2
Actual	1.35	1.37	1.44	2.05
Estimated	1.44	1.46	1.49	2.11
Error	6.67%	6.57%	3.47%	2.93%

In the experiment, the rms values of –5th-order harmonic PCC voltage, output current for both inverters are 2.12 V, 0.77 A, and 0.60 A, respectively. The estimated feeder impedance is listed in Table II. Compared with the actual feeder impedance measured by Agilent E4980A, the estimation results were sufficiently accurate.

As depicted in Fig. 8, load power-sharing error was eliminated when using the proposed method and remained acceptable even with load step changes. The power sharing performance can also be demonstrated by comparing the output current waveforms of each inverter. The output currents of phases-A and phase-B before and after inserting the virtual impedance are shown in Fig. 9. It can be seen that the output currents of both inverters differed greatly before inserting the virtual impedance as shown in Fig. 9(a); afterward, an enhanced power sharing performance was obtained by introducing proper virtual impedance as shown in Fig. 9(b), where the output currents of both inverters are almost overlapped. Fig. 10 shows that the THD of PCC voltage declined from 4.05% to 3.06% by introducing negative virtual impedance.

V. Conclusion

In this letter, a noninvasive FIEM is proposed based on the MGCC and load harmonic current in microgrids. Moreover,

$$Z_p(s) = \frac{2sL_f + 0.75V_0V_{\rm dc}Ve^{j\frac{\pi}{2}}M(s-j2\pi f)G_I(s)G_V(s)G_{md}(s) + V_{\rm dc}G_I(s)G_{md}(s)}{2+2L_fC_fs^2+0.75V_0V_{\rm dc}Ie^{j(\frac{\pi}{2}-\varphi_i)}M(s-j2\pi f)G_I(s)G_V(s)G_{md}(s)+V_{\rm dc}G_I(s)G_V(s)G_{md}(s)+sC_fV_{\rm dc}G_I(s)G_{md}(s)} \tag{A1}$$

$$Z_n(s) = \frac{2sL_f + 0.75V_0V_{\rm dc}Ve^{-j\frac{\pi}{2}}M(s+j2\pi f)G_I(s)G_V(s)G_{md}(s) + V_{\rm dc}G_I(s)G_{md}(s)}{2+2L_fC_fs^2+0.75V_0V_{\rm dc}Ie^{-j(\frac{\pi}{2}-\varphi_i)}M(s+j2\pi f)G_I(s)G_V(s)G_{md}(s)+V_{\rm dc}G_I(s)G_V(s)G_{md}(s)+sC_fV_{\rm dc}G_I(s)G_{md}(s)} \tag{A2}$$

an application example of estimated feeder impedance is introduced to enhance power sharing and voltage quality. Comprehensive experimental results are provided. The proposed method can obtain feeder impedance for parallel inverters in a noninvasive manner without extra requirements on disturbance, sensors, and communication, and power sharing and voltage quality can be effectively enhanced for microgrids. More importantly, the proposed FIEM is applicable to parallel-inverter systems under different forms of droop control and VSG control, and it also has the potential to be applied to solve other microgrid-related problems.

APPENDIX

The sequence impedance expressions of a droop-controlled inverter are shown in (A1) and (A2) shown at the top of this page, where $G_{md}(s) = e^{-1.5sT_s}$ is the PWM delay, and $M(s) = k_p\omega_{cp}/[s(s+\omega_{cp})]$ is related to droop control and LPF in power calculation

ACKNOWLEDGMENT

The authors would like to thank R. An and S. Song for their assistance with the experiment.

REFERENCES

[1] J. M. Guerrero, J. C. Vasquez, J. Matas, L. G. Vicuna, and M. Castilla, "Hierarchical control of droop-controlled AC and DC Microgrids—A general approach toward standardization," *IEEE Trans. Ind. Electron.*, vol. 58, no. 1, pp. 158–172, Jan. 2011.

[2] J. Rocabert, A. Luna, F. Blaabjerg, and P. Rodríguez, "Control of power converters in AC microgrids," *IEEE Trans. Power Electron.*, vol. 27, no. 11, pp. 4734–4749, Nov. 2012.

[3] S. Parhizi, H. Lotfi, A. Khodaei, and S. Bahramirad, "State of the art in research on microgrids: A review," *IEEE Access*, vol. 3, no. pp. 890–925, 2015.

[4] N. Hoffmann and F. W. Fuchs, "Minimal invasive equivalent grid impedance estimation in inductive–resistive power networks using extended kalman filter," *IEEE Trans. Power Electron.*, vol. 29, no. 2, pp. 631–641, Feb. 2014.

[5] J. Huang, K. A. Corzine, and M. Belkhayat, "Small-Signal impedance measurement of power-electronics-based AC power systems using Line-to-Line current injection," *IEEE Trans. Power Electron.*, vol. 24, no. 2, pp. 445–455, Feb. 2009.

[6] A. Vidal *et al.*, "A method for identification of the equivalent inductance and resistance in the plant model of current-controlled grid-tied converters," *IEEE Trans. Power Electron.*, vol. 30, no. 12, pp. 7245–7261, Dec. 2015.

[7] P. García, M. Sumner, N.-R. Á, J. M. Guerrero, and J. García, "Observer-Based pulsed signal injection for grid impedance estimation in three-phase systems," *IEEE Trans. Ind. Electron.*, vol. 65, no. 10, pp. 7888–7899, Oct. 2018.

[8] C. Liu, J. Zhao, S. Wang, W. Lu, and K. Qu, "Active identification method for line resistance in DC microgrid based on single pulse injection," *IEEE Trans. Power Electron.*, vol. 33, no. 7, pp. 5561–5564, Jul. 2018.

[9] A. Ghanem, M. Rashed, M. Sumner, M. A. Elsayes, and I. I. I. Mansy, "Grid impedance estimation for islanding detection and adaptive control of converters," *IET Power Electron*, vol. 10, no. 11, pp. 1279–1288, Nov. 2017.

[10] D. D. Reigosa, F. Briz, C. B. Charro, and J. M. Guerrero, "Passive islanding detection using inverter nonlinear effects," *IEEE Trans. Power Electron.*, vol. 32, no. 11, pp. 8434–8445, Nov. 2017.

[11] L. Wang, H. Gu, H. Ou, and X. Dou, "A voltage stability control based on impedance estimation for the independent microgrid," in *Proc. IEEE Int. Power Electron. Application Conf. Expo.*, 2018, pp. 1–5.

[12] K. Moffat, M. Bariya, and A. V. Meier, "Network impedance estimation for microgrid control using noisy synchrophasor measurements," in *Proc. IEEE 19th Workshop Control Model. for Power Electron.*, 2018, pp. 1–6.

[13] W. Wu *et al.*, "Sequence-impedance-based stability comparison between VSGs and traditional grid-connected inverters," *IEEE Trans. Power Electron.*, vol. 34, no. 1, pp. 46–52, Jan. 2019.

[14] P. Rodriguez, A. Luna, I. Candela, R. Mujal, R. Teodorescu, and F. Blaabjerg, "Multiresonant frequency-locked loop for grid synchronization of power converters under distorted grid conditions," *IEEE Trans. Ind. Electron.*, vol. 58, no. 1, pp. 127–138, Jan. 2011.

[15] J. He and Y. W. Li, "Analysis, design, and implementation of virtual impedance for power electronics interfaced distributed generation," *IEEE Trans. Ind. Appl.*, vol. 47, no. 6, pp. 2525–2538, Nov. 2011.